

# Fracture and Fatigue in Graphene Nanocomposites

Mohammad A. Rafiee, Javad Rafiee, Iti Srivastava, Zhou Wang, Huaihe Song, Zhong-Zhen Yu, and Nikhil Koratkar\*

Graphene, a single-atom-thick sheet of  $sp^2$ -bonded carbon atoms, has generated much interest due to its high specific area and novel mechanical, electrical, and thermal properties.<sup>[1–7]</sup> Recent advances<sup>[8–10]</sup> in the production of bulk quantities of exfoliated graphene sheets from graphite have enabled the fabrication of graphene–polymer composites. Such composites show tremendous potential for mechanical-property enhancement due to their combination<sup>[11–12]</sup> of high specific surface area, strong nanofiller–matrix adhesion and the outstanding mechanical properties of the  $sp^2$  carbon bonding network in graphene. Graphene fillers have been successfully dispersed in poly(styrene), poly(acrylonitrile) and poly(methyl methacrylate) matrices and the responses of their Young's modulus, ultimate tensile strength, and glass-transition temperature have been characterized.<sup>[11–12]</sup> However, to the best of our knowledge there is no report on the fracture toughness and fatigue properties of graphene–polymer composites. Fracture toughness describes the ability of a material containing a crack to resist fracture and it is a critically important material property for design applications. Fatigue involves dynamic propagation of cracks under cyclic loading and it is one of the primary causes of catastrophic failure in structural materials. Consequently, the material's resistance to fracture and fatigue crack propagation are of paramount importance to prevent failure.

Herein we report the fracture toughness, fracture energy, and fatigue properties of an epoxy polymer reinforced with various weight fractions of functionalized graphene sheets. Remarkably, only 0.125% weight of functionalized graphene sheets was observed to increase the fracture toughness of the pristine (unfilled) epoxy by  $\approx 65\%$  and the fracture energy by  $\approx 115\%$ . To achieve comparable enhancement, carbon nanotube (CNT) and nanoparticle epoxy composites<sup>[13–15]</sup> require one to two orders of magnitude larger weight fraction of nanofillers. Under fatigue conditions, incorporation of 0.125% weight of functionalized graphene sheets drastically reduced the rate of crack propagation in the epoxy  $\approx 25$ -fold. Fractography analysis

revealed that the extraordinary effectiveness of graphene to resist fracture and fatigue is related to deflection processes associated with the planar (two-dimensional) structure of graphene, which enables it to deflect cracks far more effectively than one-dimensional CNTs or low-aspect-ratio nanoparticles. Given the widespread use of epoxies in structural applications, these results are expected to translate into significant practical applications for such nanocomposite epoxies.

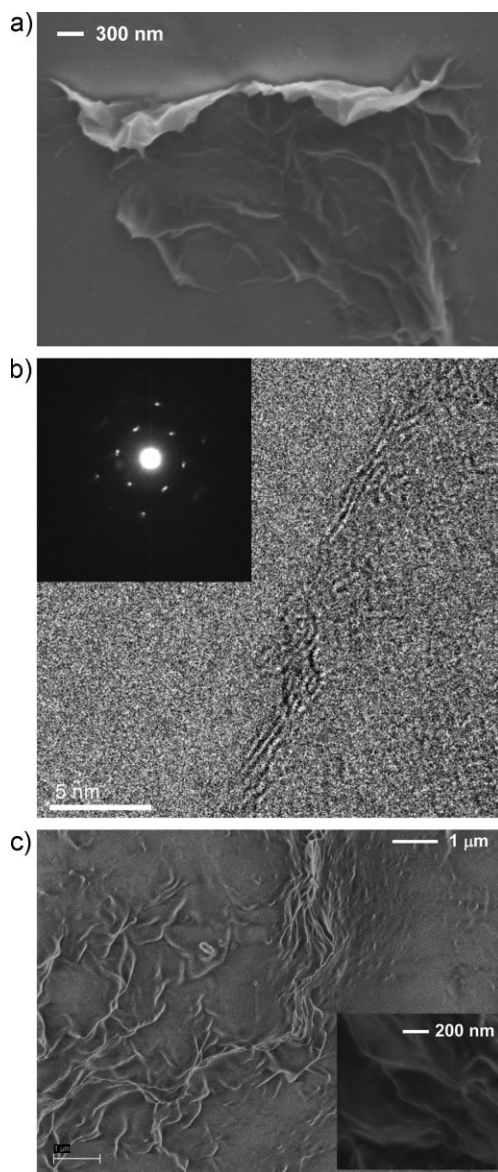
In order to synthesize bulk quantities of exfoliated graphene sheets and to effectively disperse these sheets in polymer composites we utilized a technique pioneered by Aksay and co-workers.<sup>[8,9]</sup> This method generates bulk quantities of functionalized (i.e., partially oxygenated) graphene sheets (FGS) by the rapid thermal expansion ( $>2000\text{ }^\circ\text{C min}^{-1}$ ) of completely oxidized graphite oxide. The oxygen functionalities on the graphene sheets facilitate their dispersion<sup>[10,16]</sup> in polar solvents, which makes this process convenient for composite applications. The protocols used to oxidize graphite to graphite oxide and then generate FGS by the thermal exfoliation of graphite oxide are provided in the Experimental Section and the Supporting Information (we used the same protocols as described in References [8,9]). The procedures used to disperse FGS in a bisphenol-A based thermosetting epoxy<sup>[17–19]</sup> are also described in the Experimental Section. Both compact tension samples for crack propagation study and dog-bone-shaped coupons (samples) for uniaxial tensile testing were fabricated and tested.

Figure 1a shows a scanning electron microscopy (SEM) image of a typical FGS flake synthesized by the above approach and deposited on a silicon wafer for imaging. The flake dimensions are  $\approx 4.4\text{ }\mu\text{m} \times 2.4\text{ }\mu\text{m}$ ; note the wrinkled surface texture of the FGS, which could play an important role in enhancing mechanical interlocking and load transfer with the matrix.<sup>[11,12]</sup> Figure 1b is a high-resolution transmission electron microscopy (HRTEM) image of the edge of a typical FGS flake, indicating that each flake is composed of  $\approx 2$ – $3$  individual graphene sheets. The electron diffraction pattern (shown in the inset of Figure 1b) confirms the signature of few-layered graphene.<sup>[11]</sup> Figure 1c shows an SEM image of a freeze-fractured nanocomposite sample with  $\approx 5\%$  weight of FGS. The image clearly indicates epoxy-coated FGS flakes on the fracture surface of the sample. The inset in Figure 1c depicts a high-resolution SEM image, indicating the wavy edge structure of the FGS sheets that are protruding out of the fracture surface. At low weight fractions of FGS (below 0.5%), it was quite challenging to study the FGS dispersion by SEM analysis due to the planar sheet geometry of the FGS and the epoxy coating on the FGS, which allows only the exposed sheet edges to be discerned.

[\*] Prof. N. Koratkar, M. A. Rafiee, J. Rafiee, I. Srivastava  
Department of Mechanical, Aerospace, and Nuclear Engineering  
Rensselaer Polytechnic Institute, Troy, NY 12180 (USA)  
E-mail: koratn@rpi.edu

Prof. Z.-Z. Yu, Z. Wang, H. Song  
State Key Laboratory of Chemical Resource Engineering  
College of Materials Science and Engineering  
Beijing University of Chemical Technology  
Beijing 100029 (P.R. China)

Supporting Information is available on the WWW under <http://www.small-journal.com> or from the author.



**Figure 1.** a) SEM image of a typical functionalized graphene flake deposited on a silicon wafer for imaging. b) HRTEM image of the edges of a typical graphene flake showing  $\approx 2$ – $3$  graphene layers. The inset shows the measured electron diffraction pattern, which is typical for few-layered graphene. c) SEM analysis of the freeze-fractured surface of the nanocomposite indicating epoxy-coated FGS on the fracture surface. The inset shows the wavy edges of the FGS sheets protruding out of the fracture surface.

Crack-opening tests on compact tension samples were performed to measure the Mode I fracture toughness ( $K_{Ic}$ ) of the pure epoxy matrix and the FGS–epoxy nanocomposites at various weight fractions of FGS. The tests were conducted using a MTS-858 material testing system following ASTM standard D5045 (Supporting Information). An initial pre-crack was created in the compact tension samples by gently tapping a fresh razor blade over a molded starter notch. The radius at the tip of the pre-crack was similar for all the samples tested, which was confirmed by optical microscopy prior to testing. At each weight fraction of FGS additives, we tested 4–6 different samples to

check for reproducibility of the results. Figure 2a shows that the Mode I fracture toughness ( $K_{Ic}$ ) of the baseline epoxy (without FGS) is  $\approx 1.03 \text{ MPa } \sqrt{m}$ , which correlates well with published literature<sup>[17–19]</sup> for epoxy materials. The addition of FGS into the epoxy matrix causes a sharp increase in the nanocomposite  $K_{Ic}$  value to  $\approx 1.75 \text{ MPa } \sqrt{m}$  at 0.125% weight fraction of FGS, which corresponds to a  $\approx 65\%$  increase in fracture toughness. For higher loading fractions, the enhancement in  $K_{Ic}$  diminishes (Figure 2a) and finally begins to approach the pure epoxy value at a FGS weight fraction of  $\approx 0.5\%$ . This might be a result of degradation in the dispersion of the FGS additives above a weight fraction of 0.125%. We have observed similar degradation<sup>[17–19]</sup> in the dispersion quality of CNTs in epoxy composites but at significantly larger nanotube weight fractions ( $>0.5\%$ ). Therefore, dispersion of two-dimensional FGS appears to be more challenging as compared to one-dimensional CNTs or  $\text{Al}_2\text{O}_3/\text{TiO}_2/\text{SiO}_2$  nanoparticles, which have been successfully dispersed in epoxies at very high loading fractions (up to 20%).<sup>[14,15]</sup> This is not an unexpected result given that the two-dimensional FGS (several micrometers in dimension; Figure 1a) are more easily entangled and therefore show a greater tendency to agglomerate as compared to nanoparticles or nanotubes. In spite of this, the maximum enhancement in  $K_{Ic}$  ( $\approx 65\%$  at 0.125% weight fraction of FGS) is impressive. To achieve comparable increase ( $\approx 62\%$ ) in  $K_{Ic}$ , the required weight fraction<sup>[14]</sup> ( $\approx 14.8\%$ ) of  $\text{SiO}_2$  nanoparticles in epoxy is  $\approx 120$ -fold larger than FGS. Similarly, to obtain a 65% increase in  $K_{Ic}$ , the volume fraction of  $\text{Al}_2\text{O}_3$  ( $\approx 5\%$ ) and  $\text{TiO}_2$  ( $\approx 10\%$ ) nanoparticles<sup>[15]</sup> in epoxy is  $\approx 30$ - to 60-fold larger than FGS.

Intercalated nanoclays<sup>[20–22]</sup> have also proven to be effective in toughening epoxy systems. For example, Zerda et al.<sup>[20]</sup> obtained  $\approx 61\%$  increase in fracture toughness for 3.5% nanoclay weight fraction. Wang et al.<sup>[21]</sup> obtained similar levels of  $K_{Ic}$  enhancement ( $\approx 78\%$ ) at 2.5% weight fraction of nanoclay fillers. Liu et al.<sup>[22]</sup> demonstrated  $\approx 110\%$  increase in  $K_{Ic}$  for an epoxy system with  $\approx 3\%$  weight of nanoclay additives. These weight fractions are 20–30 times higher than the FGS weight fraction of 0.125% in our study. Moreover, in the case of nanoclay epoxy composites addition of nanoclays (in the 2.5–3.5% weight fraction range) causes degradation in the tensile strength. For example, the tensile strength of the matrix<sup>[21]</sup> was reduced by 17% due to incorporation of 2.5% weight of nanoclay. Similarly the tensile strength decreased by 7.5% for 3.5% weight fraction of nanoclays in the epoxy matrix<sup>[20]</sup>. By contrast, the FGS additives were found to enhance the tensile strength by up to 45% in the 0.1–0.125% weight fraction range (Figure 2b).

For CNT–epoxy composites, the best reported enhancement<sup>[13]</sup> in  $K_{Ic}$  is  $\approx 43\%$ , which occurs at  $\approx$ fourfold-higher nanofiller weight fraction ( $\approx 0.5\%$  weight of amine-functionalized double-walled CNTs). Our recent work<sup>[17]</sup> with CNT–epoxy composites indicated  $\approx 11\%$  improvement in fracture toughness with 0.25% weight of multi-walled CNT additives. These results indicate that FGS are highly effective in suppressing crack propagation in polymer materials. However, there is a clear need to develop improved techniques for FGS dispersion in polymer matrices in order to realize their full potential. For example, pre-modifying FGS by the use of specially designed surfactants may enable enhanced dispersion at higher FGS loading fractions ( $>0.125\%$ ).

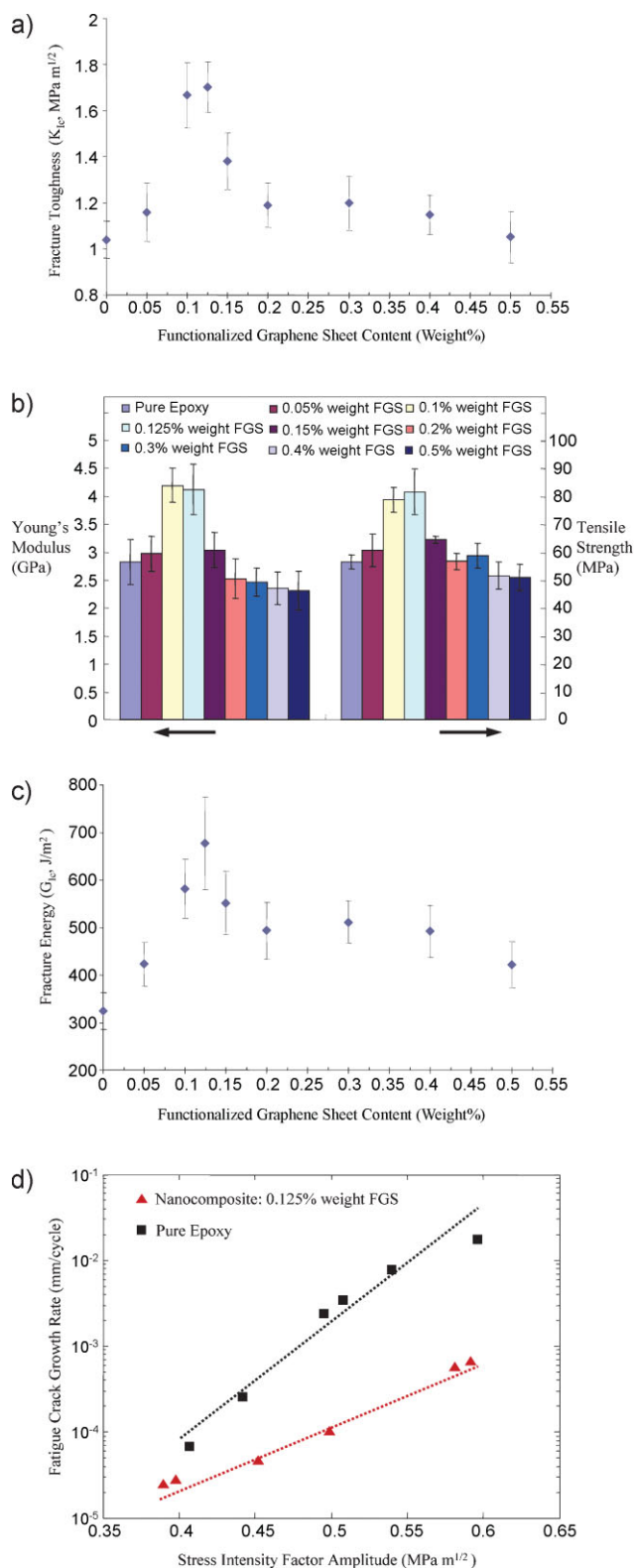


**Figure 2.** a) Mode I fracture toughness ( $K_{Ic}$ ) plotted as a function of the weight fraction of FGS in the epoxy matrix. b) Young's modulus and ultimate tensile strength of pure epoxy and nanocomposite samples with various weight fractions of FGS. c) Variation of fracture energy ( $G_{Ic}$ ) as a function of the weight fraction of FGS in the epoxy matrix. d) Fatigue crack-propagation testing; crack growth rate ( $da/dN$ ) plotted as a function of the stress intensity factor amplitude ( $\Delta K$ ) for the pristine epoxy and nanocomposite samples with 0.125% weight fraction of FGS.

We characterized the nanocomposite's Young's modulus and ultimate strength by performing tensile loading tests on dog-bone-shaped coupons. Figure 2b depicts the measured modulus for the pristine epoxy and FGS/epoxy nanocomposites. At 0.125% FGS weight fraction, the Young's modulus of the nanocomposite is  $\approx 50\%$  greater than the baseline epoxy. Figure 2b also shows the ultimate tensile strength measurements; we observe  $\approx 45\%$  enhancement in the ultimate tensile strength at 0.125% weight fraction of FGS. In contrast, CNTs show  $\approx 30\%$  increase in modulus and  $\approx 15\%$  increase in strength for 1% weight of functionalized single-walled CNTs in epoxy.<sup>[23]</sup> Therefore, compared to CNTs, FGS imparts superior tensile strength and stiffness properties to the epoxy matrix at nearly an order of magnitude lower nanofiller weight fraction. This is indicative of improved mechanical interlocking and adhesion between the FGS and the polymer matrix, which may result from the rough and wrinkled texture of FGS (Figure 1a). Distortions caused by oxygen functionalization and the resultant defects during thermal exfoliation of graphite oxide, as well as the extremely small thickness of FGS, lead to a wrinkled topology at the nanoscale.<sup>[12]</sup> This nanoscale surface roughness likely results in enhanced mechanical interlocking with the polymer chains and, consequently, better adhesion. Such an effect has also been suggested by recent molecular dynamics studies.<sup>[24–25]</sup> The glass-transition temperature of the FGS–epoxy nanocomposite was also significantly elevated in comparison to the pristine epoxy (Supporting Information); this could result from enhanced adhesion<sup>[11,12]</sup> at the FGS–matrix interface as well as conformational changes<sup>[26,27]</sup> to the epoxy polymer in the vicinity of the FGS.

The measurement of modulus ( $E$ ) and fracture toughness ( $K_{Ic}$ ) enables us to compute the critical energy release rate,  $G_{Ic} = K_{Ic}^2 \frac{(1-\nu^2)}{E}$ , where  $\nu$  is the Poisson ratio. The fracture energy ( $G_{Ic}$ ) quantifies the energy required to propagate the crack in the material. Figure 2c indicates that the  $G_{Ic}$  of the baseline epoxy (without FGS) is  $\approx 325 \text{ J m}^{-2}$ , which correlates well with published literature<sup>[28]</sup> for brittle polymers, which typically show  $G_{Ic}$  less than  $500 \text{ J m}^{-2}$ . Incorporation of FGS into the epoxy causes a large increase in the nanocomposite's  $G_{Ic}$  to  $\approx 700 \text{ J m}^{-2}$  at 0.125% weight fraction of FGS, which corresponds to a  $\approx 115\%$  increase. The critical energy release rate for the FGS–epoxy nanocomposite is comparable to brittle metals, which typically display  $G_{Ic}$  in the range of  $800\text{--}2000 \text{ J m}^{-2}$ .

To evaluate the nanocomposite's performance in fatigue environments, dynamic crack-propagation tests were performed on compact tension samples using ASTM standard E647 (details provided in the Supporting Information). Figure 2d shows the measured crack-propagation rate ( $da/dN$ ) versus the applied stress intensity factor amplitude ( $\Delta K$ ) for the baseline epoxy and the nanocomposite with 0.125% weight fraction of FGS. The weight fraction was not increased beyond 0.125% since it is challenging to maintain FGS dispersion at higher loading fractions. The results indicate a significant reduction in crack growth rate for the nanocomposite compared to the pristine epoxy over the full range of stress intensity factor amplitudes that were tested. For example, at  $\Delta K = 0.5 \text{ MPa } \sqrt{\text{m}}$ , the  $da/dN$  for the nanocomposite ( $1.0165 \times 10^{-4} \text{ mm/cycle}$ ) is  $\approx 25$  times lower than the baseline

epoxy ( $2.49 \times 10^{-3}$  mm/cycle). We fitted the crack growth results (Figure 2d) to the Paris–Erdogan law:  $\frac{da}{dN} = C(\Delta K)^n$ . We find a significant reduction in the exponent  $n$  (from  $\approx 17.33$  to  $\approx 7.94$ ) and the constant  $C$  (from  $\approx 394.26$  to  $\approx 0.0358$ ) for the nanocomposite compared to the baseline epoxy.

To develop an understanding of the enhanced ability of FGS to resist fracture and fatigue, we performed fractography analysis of the fracture surface of the compact tension samples tested in the study. SEM analysis of the fracture surface (Supporting Information) did not reveal any direct evidence of crack pinning or crack bridging by the FGS additives. However, we observed a significant increase in average surface roughness of the fracture surface with FGS content, as indicated in Figure 3a. The average surface roughness ( $R_a$ ) of the fracture surfaces was measured using a Dektak Surface Profiler (from VEECO); at least 6 separate measurements were performed for each sample for statistics. The data indicates a doubling in the average surface roughness with increase in FGS content from 0 to 0.125% weight. This roughening effect begins to saturate with further increase in the FGS content. The increasing roughness of the fracture surface with FGS content suggests that crack deflection appears to play a significant role in the observed toughening. Crack deflection is the process by which an initial crack tilts and twists when it encounters a rigid inclusion. This generates an increase in the total fracture surface area, resulting in greater energy absorption as compared to the unfilled polymer material. The tilting and twisting of the crack front as it is forced to move out of the initial propagation plane also forces the crack to grow locally under mixed-mode (tensile/in-plane shear and tensile/anti-plane shear) conditions. Crack propagation under mixed-mode conditions requires a higher driving force than in Mode I (tension), which also results in higher fracture toughness of the material. If such crack deflection processes play a major role then we expect a linear increase<sup>[28,29]</sup> in the fracture surface roughness ( $R_a$ ) as the fracture energy ( $G_{Ic}$ ) is increased. This indeed appears to be the case in the 0–0.125% FGS weight fraction range, as indicated in Figure 3b. However, for higher weight fractions the trend reverses, which suggests that a competing mechanism (probably agglomeration of FGS) that decreases the fracture toughness comes into play.

To understand why crack deflection may be more effective for high-aspect-ratio FGS sheets as compared to conventional fillers, we used the classical Faber and Evans model<sup>[30]</sup> for crack deflection. In the Supporting Information we show the normalized toughening increment generated by crack tilting versus the particle aspect ratio (as predicted by the Faber and Evans model) for particles with rod, sphere, and plate geometries. The results (Supporting Information) indicate that for plates with large aspect ratio (such as an FGS sheet), the tilting of the crack front acts as a significant source of toughening. It is also evident that neither the sphere nor the rod-shaped particles derive noticeable toughening from the crack tilting process. Furthermore, the aspect ratio of the rod has little effect on the toughening during the crack tilt process. This indicates that the FGS sheet geometry with its very large aspect ratio is expected to be highly effective in toughening the matrix, which is consistent with our experimental observations.

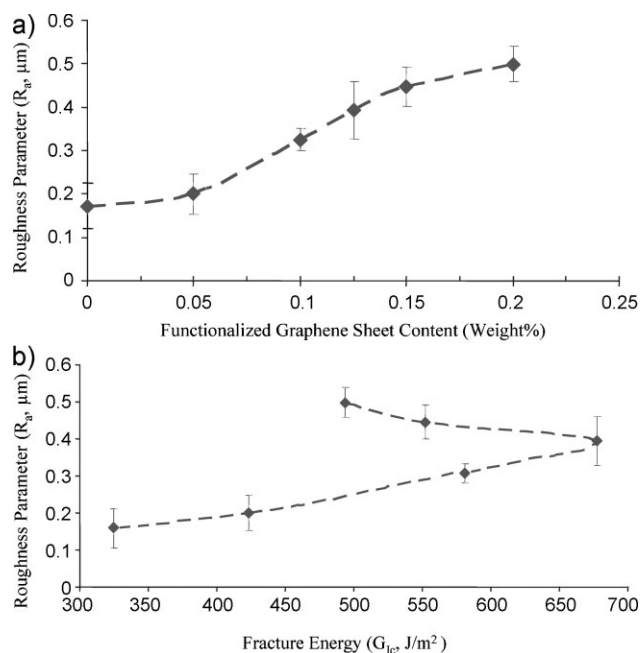


**Figure 3.** a) Fracture surface roughness parameter ( $R_a$ ) plotted as a function of the weight fraction of FGS in the epoxy matrix. b) Variation in  $R_a$  as a function of the fracture energy ( $G_{Ic}$ ). The linear increase of  $R_a$  with  $G_{Ic}$  (in the 0–0.125% FGS weight fraction range) indicates that crack deflection processes appear to play a significant role in the toughening of the FGS/epoxy nanocomposite.

In summary, functionalized graphene sheets are remarkably effective at enhancing the fracture toughness, fracture energy, stiffness, strength, and fatigue resistance of epoxy polymers at significantly lower nanofiller loading fractions in comparison to CNTs, nanoparticles, and nanoclay additives. This can be attributed to their enhanced specific surface area, two-dimensional geometry, and strong nanofiller-matrix adhesion. However, improved techniques to quantify the dispersion of graphene in polymer matrices and enhanced dispersion of graphene sheets at high nanofiller loading fractions are necessary to realize the full potential of graphene-based composite materials.

## Experimental Section

Natural graphite flakes with an average diameter of  $48 \mu\text{m}$  were supplied from Huadong Graphite Factory (Pingdu, China). Concentrated sulfuric acid (95–98%), concentrated nitric acid (68%) and hydrochloric acid (36–38%) were purchased from Beijing Chemical Factory, China. Potassium chlorate (99.5%) was obtained from Fuchen Chemical Reagents (Tianjin, China). The epoxy used in the present study was a Bisphenol-A-based epoxy (Epoxy 2000 from Fibreglast, USA) and the curing agent used was 2120 Epoxy Hardener from Fibreglast, USA.

**FGS fabrication:** Graphite oxide was prepared by oxidizing graphite in a solution of sulfuric acid, nitric acid, and potassium chlorate for 96 hours based on the work of Aksay and co-workers.<sup>[8,9]</sup> X-ray diffraction patterns of natural graphite and graphite oxide are provided in the Supporting Information. Thermal exfoliation of graphite oxide was achieved by placing the graphite oxide powder (200 mg) in a 200-mm-inner-diameter, 1-m-long quartz tube that was sealed at one end. The other end of

the quartz tube was closed using a rubber stopper. An argon inlet was then inserted through the rubber stopper. The sample was flushed with argon for 10 min, and the quartz tube was quickly inserted into a tube furnace (Thermolyne 79300, Thermo Fisher Scientific Inc., USA) preheated to 1050 °C and held in the furnace for 30 s. Rapid heating (>2000 °C min<sup>-1</sup>) splits the graphite oxide into functionalized graphene sheets (FGS) through the evolution of CO<sub>2</sub> gas as demonstrated in References [8, 9].

*Dispersion of FGS in epoxy matrix:* The desired amount of FGS was first weighed and dispersed in acetone (ratio of 100 mL of acetone to 0.1 g of FGS) using an ultrasonic probe sonicator at high amplitude (Sonics Vibracell VC 750, Sonics and Materials Inc., USA) for 1.5 h in an ice bath. The epoxy (System 2000 Epoxy Resin, Fibreglast Inc, USA) was added to the mixture and sonicated following the same procedure for another 1.5 h. Next, the acetone was evaporated off by heating the mixture on a magnetic stir plate using a Teflon-coated magnetic bar for 3 h at 70 °C. Subsequently, the mixture is placed in a vacuum chamber for 12 h at 70 °C to ensure that all of the acetone had been removed. After allowing the FGS/epoxy slurry to cool down to room temperature to prevent any premature curing, a low-viscosity curing agent (2120 Epoxy Hardener, Fibreglast Inc, USA) was added and mixed using a high-speed shear mixer (ARE-250, Thinky, Japan) for 4 min at 2000 rpm. The mixture was again placed in a vacuum chamber to degas the epoxy for approximately 30 min. Finally, the mixture was poured into Silicon moulds and the nanocomposite was cured at room temperature and 90 psi pressure for 24 h, followed by 4 h of post cure at 90 °C.

## Acknowledgements

N.K. acknowledges funding support from the US Office of Naval Research (Award Number: N000140910928) and the US National Science Foundation (Award Number: 0900188).

## Keywords:

graphene · nanocomposites · fractures · fatigue

- 
- [1] D. Li, R. B. Kaner, *Science* **2008**, *320*, 1170.  
 [2] K. N. Kudin, B. Ozbas, H. C. Schniepp, R. K. Prud'homme, I. A. Aksay, *Nano Lett.* **2008**, *8*, 36.  
 [3] A. K. Geim, K. S. Novoselov, *Nat. Mater.* **2007**, *6*, 183.  
 [4] F. Schedin, A. K. Geim, S. V. Morozov, E. W. Hill, P. Blake, M. I. Katsnelson, K. S. Novoselov, *Nat. Mater.* **2007**, *6*, 652.  
 [5] D. C. Elias, R. R. Nair, T. H. G. Mohiuddin, S. V. Morozov, P. Blake, M. P. Halsall, A. C. Ferrari, D. W. Boukhvalov, M. I. Katsnelson, A. K. Geim, K. S. Novoselov, *Science* **2009**, *323*, 610.  
 [6] S. Y. Zhou, G.-H. Gweon, A. V. Fedorov, P. N. First, W. A. De Heer, D.-H. Lee, F. Guinea, A. H. Castro Neto, A. Lanzara, *Nat. Mater.* **2007**, *6*, 770.  
 [7] C. Lee, X. Wei, J. W. Kysar, J. Hone, *Science* **2008**, *321*, 385.  
 [8] H. C. Schniepp, J.-L. Li, M. J. McAllister, H. Sai, M. Herrera-Alonso, D. H. Adamson, R. K. Prud'homme, R. Car, D. A. Saville, I. A. Aksay, *J. Phys. Chem. B* **2006**, *110*, 8535.  
 [9] M. J. McAllister, J.-L. Li, D. H. Adamson, H. C. Schniepp, A. A. Abdala, J. Liu, M. Herrera-Alonso, D. L. Milius, R. Car, R. K. Prud'homme, I. A. Aksay, *Chem. Mater.* **2007**, *19*, 4396.  
 [10] S. Stankovich, R. D. Piner, S.-T. Nguyen, R. S. Ruoff, *Carbon* **2006**, *44*, 3342.  
 [11] S. Stankovich, D. A. Dikin, D. Dommett, K. Kohlhaas, E. J. Zimney, E. A. Stach, R. D. Piner, S. T. Nguyen, R. S. Ruoff, *Nature* **2006**, *442*, 282.  
 [12] T. Ramanathan, A. A. Abdala, S. Stankovich, D. A. Dikin, M. Herrera-Alonso, R. D. Piner, D. H. Adamson, H. C. Schniepp, X. Chen, R. S. Ruoff, S. T. Nguyen, I. A. Aksay, R. K. Prud'homme, L. C. Brinson, *Nat. Nanotechnol.* **2008**, *3*, 327.  
 [13] F. H. Gojny, M. H. G. Wichmann, B. K. Fiedler, K. Schulte, *Comp. Sci. Technol.* **2005**, *65*, 2300.  
 [14] B. R. K. Blackman, A. J. Kinloch, J. Sohn Lee, A. C. Taylor, R. Agarwal, G. Schueneman, S. Sprenger, *J. Mater. Sci.* **2007**, *42*, 7049.  
 [15] B. Wetzels, P. Rosso, F. Hauptert, K. Friedrich, *Eng. Fract. Mech.* **2006**, *73*, 2375.  
 [16] S. Park, J. A. An, I. Jung, R. D. Piner, S. J. An, X. Li, A. Velamakanni, R. S. Ruoff, *Nano Lett.* **2009**, *9*, 1593.  
 [17] W. Zhang, I. Srivastava, Y.-F. Zhu, C. R. Picu, N. Koratkar, *Small* **2009**, *5*, 1403.  
 [18] W. Zhang, C. R. Picu, N. Koratkar, *Appl. Phys. Lett.* **2007**, *91*, 193109.  
 [19] W. Zhang, C. R. Picu, N. Koratkar, *Nanotechnology* **2008**, *19*, 285709.  
 [20] A. S. Zerda, A. J. Lesser, *J. Polym. Sci. Pol. Phys.* **2001**, *39*, 1137.  
 [21] K. Wang, L. Chen, J. Wu, M. L. Toh, C. He, A. F. Yee, *Macromolecules* **2005**, *38*, 788.  
 [22] W. Liu, S. V. Hoa, M. Pugh, *Compos. Sci. Technol.* **2005**, *65*, 2364.  
 [23] J. Zhu, J. Kim, H. Peng, J. L. Margrave, V. N. Khabashesku, E. V. Barrera, *Nano Lett.* **2003**, *3*, 1107.  
 [24] F. W. Starr, T. B. Schroder, S. C. Glotzer, *Macromolecules* **2002**, *35*, 4481.  
 [25] G. D. Smith, D. Bedrov, L. W. Li, O. Bytner, *J. Chem. Phys.* **2002**, *117*, 9478.  
 [26] V. A. Harmandaris, K. C. Daoulas, V. G. Mavrantzas, *Macromolecules* **2005**, *38*, 5796.  
 [27] T. Desai, P. Keblinski, S. K. Kumar, *J. Chem. Phys.* **2005**, *122*, 134910.  
 [28] D. Hull, *Fractography: observing, measuring, and interpreting fracture surface topography*, Cambridge University Press, Cambridge **1999**.  
 [29] K. Arakawa, K. Takahashi, *Int. J. Fract.* **1991**, *48*, 103.  
 [30] K. T. Faber, A. G. Evans, *Acta. Metall. Mater.* **1983**, *31*, 565.

Received: August 10, 2009  
 Revised: October 12, 2009  
 Published online: November 18, 2009